RNA-binding properties and membrane insertion of *Melon necrotic spot virus* (MNSV) double gene block movement proteins

J. A. Navarro[1], A. Genovés[1], J. Climent[1], A. Saurí[2], L. Martínez-Gil[2], I. Mingarro[2] and V. Pallás[1]

[1] Instituto de Biología Molecular y Celular de Plantas, Universidad Politécnica de Valencia-CSIC, Avenida de los Naranjos s/n, 46022 Valencia, Spain.

[2] Departament de Bioquímica i Biologia Molecular, Universitat de València. 46100 Burjassot, València, Spain.

Corresponding author address:

Dr. Vicente Pallás

Instituto de Biología Molecular y Celular de Plantas (IBMCP). UPV-CSIC, Av. De los Naranjos, s/n. 46022, Valencia, Spain.

Telephone: 34 963877877, FAX: 34 963877859, e-mail: vpallas@ibmcp.upv.es

ABSTRACT

Advances in structural and biochemical properties of carmovirus movement proteins (MPs) have only been obtained in p7 and p9 from *Carnation mottle virus* (CarMV). Alignment of carmovirus MPs revealed a low conservation of amino acid identity but interestingly, similarity was elevated in regions associated with the functional secondary structure elements reported for CarMV which were conserved in all studied proteins. Nevertheless, some differential features in relation with CarMV MPs were identified in those from *Melon necrotic virus* (MNSV) (p7A and p7B). p7A was a soluble non-sequence specific RNA-binding protein, but unlike CarMV p7, its central region alone could not account for the RNA-binding properties of the entire protein. In fact, a 22-amino acid synthetic peptide whose sequence corresponds to this central region rendered an apparent dissociation constant (K_d) significantly higher than that of the corresponding entire protein (9 mM *vs* 0.83-25.7 μM). This p7A-derived peptide could be induced to fold into an alpha-helical structure as demonstrated for other carmovirus p7-like proteins. Additionally, *in vitro* fractionation of p7B transcription/translation mixtures in the presence of ER-derived microsomal membranes strongly suggested that p7B is an integral membrane protein. Both characteristics of these two small MPs forming the double gene block (DGB) of MNSV are discussed in the context of the intra- and inter- cellular movement of carmovirus.

Keywords: MNSV, Melon plants, RNA binding domain, membrane insertion, movement proteins.

INTRODUCTION

Cell-to-cell movement of plant viruses requires specific viral factors (movement proteins, MP) that direct virus transport from the primary infection point to neighbouring cells by interacting with either entire viral particles (Pouwels *et al*., 2004) or nucleoprotein intermediates, including active replication complexes (Kawakami *et al*., 2004). These viral or subviral particles are commonly targeted by the machinery of the intracellular transport of macromolecules to the cell periphery where plant viruses overcome the rigid cell wall barrier by moving through modified intercellular channels (plasmodesmata), most likely by means of an internal membranous translocation system. Consequently, MPs have inevitably been found to associate with cytoskeletal elements or endoplasmic reticulum network as well as host factors in order to assist the movement process (Heinlein and Epel, 2004; Nelson and Citovsky, 2005, Lucas, 2006). Moreover, they are forced to adjust plasmodesmata dimensions to that of the viral mobile element by increasing their size exclusion limit (Waigmann *et al*., 2004). Alternatively, they can cause a drastic rearrangement of the original structure that is occasionally replaced by specialized MP-tubules (Kasteel *et a*l., 1997). Given existing data, it is evident that MPs play a central role in the spread of infection by accomplishing several functions: 1) viral genome binding (Citovsky *et al*., 1990; Marcos *et al*, 1999; Herranz and Pallas, 2004); 2) association with the intracellular transport pathway and related host factors (Lucas, 2006); 3) interaction with additional MPs or with different viral factors such as coat protein (Sanchez-Navarro *et al*, 2005 Verchot-Lubicz, 2005); 4) plasmodesmata gating (Wolf *et al*., 1989), and 5) influencing RNA silencing suppression (Bayne *et al*, 2005; Genoves *et al*., 2006). It has been reported that an individual MP may mediate most of the above mentioned activities. Otherwise, a distribution of these functions among multiple viral proteins is also possible. In this sense, five different virus-specific systems for cell-to-cell movement have been described: 1) the extensively characterized “30K superfamily” present in a large number of plant viruses representing a unique MP that shows structural similarities to the 30 kDa MP of *Tobacco mosaic virus*, TMV (Melcher, 2000); 2) the tymovirus MP (Bozarth *et al*., 1992); 3) the two small MPs encoded by carmo-like viruses (Li *et al.*, 1998; Vilar *et al*, 2001; Genoves *et al*., 2006) referred to as the double gene block proteins (DGBp; Hull, 2002) and the two MPs encoded by some geminiviruses (nuclear shuttle protein, NSP and movement protein, MP) (Noueiry *et al.*, 1994; Sanderfoot and Lazarowitz, 1995); 4) the triple gene block of proteins from potexviruses (Morozov and Solovyev, 2003; Verchot-Lubicz, 2005); and 5), filamentous closteroviruses which require up to five proteins for cell-to-cell movement (CP, minor CP, and three MPs, namely the 6-kDa protein, the Hsp70 homolog, and the 64-kDa protein) (Prokhnevsky *et al*., 2002; Peremyslov *et al*., 2004).

Coordination between two small proteins (smaller than 10kDa) encoded in the central region of the non-segmented plus stranded RNA genome of carmoviruses allows for the movement of both *Turnip crinkle virus* (TCV) as well as *Melon necrotic spot virus* (MNSV) genomes among adjacent cells (Hacker *et al.*, 1992; Li *et al.*, 1998; Cohen *et al*., 2000; Genoves *et al*., 2006). However, structural and molecular properties involving this simple movement apparatus have only been studied for the homologous MP of *Carnation mottle virus* (CarMV). CarMV p7 presents three different putative domains. However, only the basic central region, which adopts an α-helical conformation in the presence of secondary structure inducers, is responsible for the RNA binding properties (Marcos *et al*, 1999; Vilar *et al*, 2001 and 2005). On the other hand, CarMV p9 contains two transmembrane domains (TM1 and TM2) (Vilar *et al*., 2002) that are *in vitro* targeted and inserted into ER-derived microsomes by means of a cotranslational/signal recognition particle (SRP)-dependent and translocon-assisted process (Sauri *et al*., 2005). Based on these data, a topological model has been proposed in which CarMV p9 is anchored to the membrane with its N- and C-terminal regions oriented to the cytoplasmic face and with its C-terminus interacting with the soluble, RNA-bound p7 partner (Vilar *et al*., 2002). However, data involving both p7 and p9 proteins in CarMV cell-to-cell movement *in vivo* are lacking.

Here we provide a structural study of homolog DGB proteins from all sequenced carmoviruses and demonstrate the *in vitro* RNA-binding capacity and membrane insertion ability of MNSV p7A and p7B, respectively. Characterized properties of both p7A and p7B demonstrate adaptation to their assigned role in MNSV cell-to-cell movement *in vivo* (Genoves *et al*., 2006), which represents a step forward towards definition of reliable molecular models for DGBp-mediated cell-to-cell movement of plant viruses.

RESULTS

Sequence alignment and structural properties of homologous proteins from the carmovirus double gene block movement proteins (DGBp). Secondary structure prediction by computer-assisted methods and alignment of amino acid sequences were carried out with homologous DGBp from eleven carmoviruses as well as from the related *Pelargonium line pattern virus* (PLPV, Castano and Hernandez, 2005) as a reevaluation of the studies previously performed (Marcos *et al*., 1999; Cañizares *et al*, 2001; Vilar *et al*, 2001, 2002). For the 5' distal protein (referred here as DBGp1), the accuracy of prediction approaches were confirmed by a reasonable correlation between the consensus secondary structure of p7 CarMV obtained from data of six different computational prediction methods (PHDpsi, PROFsec, SSPro 2.01, Predator, YASPIN, JNet and PSIPred) by means of SYMPRED server (http://ibivu.cs.vu.nl/programs/sympredwww/) and that deduced experimentally by means of circular dichroism spectroscopy analyses (Vilar *et al*, 2001, 2002, 2005). Three different structured domains were assumed: an unordered N-terminus, an inducible α-helical central region and a C-terminus with potential β-sheet folding. The presence of these secondary structure elements mapping in the homologous positions were predicted in all studied proteins (Figure 1a). Moreover, alignment of amino acid sequences computed by means of Clustal X (1.8) interface (Thompson *et al*., 1997) revealed low sequence identity among all proteins at the N-terminus. However, the central and Ct-domains exhibited a moderate and high degree of similarity respectively, concordant with the prediction of secondary structure elements. These data suggested a conservation of amino acid properties as well as primary sequence mainly when the protein structure was affected. The α-helical structure located at the central region was variable depending on the virus, but always included a 3' distal α-helix similar to that characterized in the p7 CarMV segment ^{29}AKDAIRK^{35} (Vilar *et al*. 2001, 2005). This motif was also preceded by several conserved basic residues which confer a surrounding positive charge density distribution (Figure 1a). It has been demonstrated that this domain is responsible for the RNA binding properties of intact CarMV p7 by means of a RNA-protein adaptative interaction process modulated by the above mentioned secondary structure element (Marcos *et al*., 1999; Vilar *et al*, 2001 and 2005). Interestingly, most of the acidic residues are located at the N-terminus of the protein, resulting in a negative overall charge allocation, except for MNSV, PSNV, CPMoV, CCFV and PLPV, where positively-charged residues were found at the N-terminus and central region (Figure 1a). Finally, well-defined Ct β-sheet folding was predicted in all cases.

The amino acid sequence from 3' distal homolog proteins (DGBp2) were analyzed for possible

transmembrane (TM) segments with the aid of TMHMM (Krogh et al., 2001), DAS (Cserzö et al., 1997), HMMTOP (Tusnady and Simon, 1998) and TopPredII (Claros and von Heijne, 1994). Consensus domains are presented in Figure 1b. Homologs DGBps2 show a high percentage of hydrophobic amino acids distributed along either one or two predicted TM α-helices (TMH), arranging the proteins into two different groups that we refer to as CarMV-like (Figure 1b, upper group) and MNSV-like (Figure 1b, lower group). A conserved β-sheet structure was predicted at the C-terminus of both groups, most likely involved in the interaction with the similar motif at the C-terminus of DGBp1 (Vilar *et al*, 2001). As previously observed with DGBp1, homologs of DGBp2 show an overall low sequence identity, although regions with moderate similarity are associated with the presence of TMH. Interestingly, both TMH from CarMV-like DGBp2 are separated by a polar region containing several proline residues (Figure 1b, up). The cyclic structure of this amino acid strongly restricts the conformational space of the peptide chain in protein structures and tends to inhibit both α-helical and β-sheet structure formation. This probably forces the proteins to fold as helical hairpins. In this sense, it has been recently shown that this short loop ensures that, after translation, both TMH fragments from CarMV p9 leave the translocon complex in a concerted fashion to become membrane embedded (Saurí *et al*., 2005).

RNA-binding properties of MNSV p7A. A relationship between DGBps and carmovirus cell-to-cell movement cab be inferred by sequence similarity with DGBp from TCV and MNSV, the two carmoviruses where these proteins have been shown to be directly involved in *in vivo* cell-to-cell movement (Hacker *et al.*, 1992; Li *et al.*, 1998; Cohen *et al*., 2000; Genoves *et al*., 2006). However, DGBp from MNSV have some different structural features compared with well-characterized CarMV DGBp: the 5' distal protein (p7A) shows a different distribution of positive charge residues, and only one membrane spanning domain was predicted for DGBp2 (p7B). Therefore, to investigate whether the CarMV DGBp properties (Marcos *et al*., 1999; Vilar *et al*, 2001and 2002) are assumed by homolog MNSV proteins, studies on both *in vitro* p7A RNA binding properties as well as p7B membrane insertion were performed.

The putative RNA-binding properties of the p7A movement protein were studied by *in vitro* EMSA (Herranz and Pallas, 2004) using increasing amounts of a recombinant protein expressed in bacteria consisting of the p7A fused at the N terminus with maltose binding protein (MBP-p7A), and a MNSV-specific DIG-labelled ssRNA (CP(+) RNA) (Figure 2a, left). RNA mobility shifts, suggesting the presence of an RNA-protein interaction, became detectable when 400 ng of MBP-p7A protein was added to the reaction mixture. Maximal binding occurred using 6 μg of protein, as measured by disappearance of unbound RNA.

Comparable concentrations of MBP-βgalα protein expressed in bacteria containing the empty pMal-c2x vector failed to bind CP(+) RNA, indicating that the shift observed in the EMSAs was specific for p7A (data not shown). Interestingly, the MBP-p7A:RNA complexes formed at higher protein amounts slightly increased the electrophoretical mobility of the ribonucleoprotein complex, which at lower protein amounts (between 0.4-6 μg), migrated only slightly into the gel matrix. Similar results have been previously reported for *Prunus necrotic ringspot virus* MP indicating that the higher protein amounts the greater protein-protein interactions that result in a structural change of the ribonucleoprotein complex from rod-like to a globular form (Herranz and Pallas, 2004). Alternatively, a His-tagged p7A was used in *in vitro* EMSA. As expected from the previous experiments performed with the fusion protein MBP-p7A, RNA mobility shift was also detected although in this case, intermediate complexes were observed (supplementary figure 1a).

Binding kinetics analysis was performed using a Hill transformation of data from three independent experiments using both MBP-p7A and His-tagged p7A (Figure 2a, right and supplementary figure 1b, respectively). RNA-protein complex formation was measured as the disappearance of the band corresponding to unbound CP(+) RNA from each EMSA (Carey, 1991; Daros and Carrington, 1997). The apparent dissociation constants (K_d) for both MBP-p7A: RNA and His-tagged p7A: RNA complexes were calculated from linear regression as the p7A concentration at which half of the RNA is bound. These values (25.7 μM and 0.82 μM, respectively). were in the same order as those corresponding to homolog CarMV p7 (2.4 μM) (Marcos *et al*., 1999; Vilar *et a*l, 2001) as well as to other sequence non-specific RNA-binding proteins (Burd and Dreyfuss, 1994; Pata *et al*., 1995; Skuzeski and Morris, 1995; Daros and Carrington, 1997; Herranz and Pallas, 2004). Additionally, Hill plot of the data provides a mathematical calculation of the degree of cooperativity in the binding event, which is provided by the gradient of the resulting line or Hill coefficient (c). The c values for MBP-p7A:RNA and His-tagged p7A binding kinetics were slightly higher than 1 (c=1.1and 1.3, respectively). Therefore, a low degree of cooperativity could be assigned to the process (c=1 is indicative of no cooperativity) suggested by the presence of intermediates complexes in the EMSA performed with the His-tagged p7A (supplementary figure 1a) (Marcos *et al*, 1999). The size of MBP moiety present in the fusion protein MBP-p7A may affect p7A-p7A interactions so that decreasing the c value and perhaps, avoiding also the appearance of intermediate complexes.

To challenge the forces that govern the MBP-p7A:RNA interaction, complex resistance was evaluated by increasing NaCl concentration of the incubation mixtures in the presence of a protein concentration (6 μg) that was sufficient to bind all CP (+) RNA molecules. The appearance of free RNA was quantified to evaluate

complex dissociation and a 50% reduction of binding was observed at NaCl concentration of 435 mM (IC50) (Figure 2b, left). This remarkable salt tolerance was similar to that observed with homolog TCV p8 (Wobbe *et al*., 1998) suggesting that interactions other than electrostatics between the RNA and the MP are involved in binding (Herranz and Pallas, 2004). These results are in contrast with those obtained in similar assays but using a recombinant protein consisting of the MNSV p7B fused at the N terminus with MBP (MBP-p7B) (supplementary figure 2). Free RNA consistently disappeared only at a NaCl concentration of 50 mM. Putative interaction was unstable at any other salt concentration most likely indicating an artefactual RNA binding.

Finally, competitive binding assays were performed to examine the selectivity of p7A to bind different nucleic acids (Figure 2b, right). Reaction mixtures containing the DiG-labelled CP(+) ssRNA were assembled in the presence of a 10-fold mass excess of unlabelled competitors. The ssRNA from a heterologous origin (*Lettuce big vein virus*; LBVV; Navarro *et al*., 2004) was able to compete at 10-fold excess (Figure 2b, lanes 3 and 4), whereas the dsDNA weakly displaced the binding only at a 10-fold ratio (Figure 2b, lanes 9 and 10). Both dsRNA and ssDNA had no effect on the electrophoretic retardation (Figure 2b, lanes 5 to 8). These results indicated that the p7A has a preference for ssRNA binding in a sequence non-specific manner.

Characterization of the RNA-binding domain of p7A MP. Three deletion variants lacking each of the previously mentioned p7A structural regions (Figure 3a) were expressed as MBP fusion proteins to avoid incorrect conformation after denaturation and refolding (Citovsky *et al.,* 1992; Vaquero *et al.,* 1997) in Northwestern assay (Aparicio *et al*., 2003, Herranz and Pallas, 2004). Recombinant MBP-p7A$\Delta_{1\text{-}22}$ and MBP-p7A$\Delta_{45\text{-}65}$, deficient in the N-terminal and C-terminal domains respectively, showed strong reduction of RNA binding activity when compared with full-length MBP-p7A (Figure 3b, compare lane 2 with 4 and 6). However, deletion of the basic α-helical predicted domain located in the central portion of the protein (mutant MBP-p7A$\Delta_{23\text{-}44}$) eliminated RNA:protein interaction (Figure 3b, lane 5). No binding of the riboprobe was observed with MBP-βgalα protein (Figure 3b, lane 3). This p7A RNA binding domain (RBD) fits well with the previously described RBD from p7 CarMV (Marcos *et al*., 1999; Vilar *et al*, 2001, 2005). To corroborate these results a 22-amino acid synthetic peptide covering p7A positions 23 to 44 was synthesized. This p7A derived peptide (p7A$_{23\text{-}44}$) was randomly structured in aqueous solution as monitored through far-UV circular dichroism spectroscopy. However, increasing concentrations of secondary structure inducers, such as trifluorethanol (TFE) (Figure 4a, left panel) and SDS (Figure 4a, right panel) induced p7A$_{23\text{-}44}$ to fold into an α-helical conformation. *In vitro* RNA-binding properties of p7A$_{23\text{-}44}$ peptide were demonstrated by EMSA and

the kinetics of the process was evaluated by the same approach used with the MBP-p7A protein (Figure 4b). K_d from $p7A_{23-44}$ peptide was higher than that observed for the MBP-p7A protein (9 mM *vs* 25.7μM, respectively).

p7B is an integral membrane protein. Computer analysis of the p7B amino acid sequence predicted that p7B is a membrane protein with a single transmembrane domain, roughly spans from residue 14 to residue 32. To test the computer predictions, *in vitro* p7B transcription/translation experiments were performed in the presence of ER-derived microsomal membranes. After centrifugation of the translation reaction mixture, p7B was recovered from the 100.000 g pellet fraction (Figure 5a, untreated lanes) indicating that it could be either a membrane-associated (peripheral or integral) protein or a luminal protein (Figure 5b). To differentiate between these possibilities, translation reaction mixtures were either treated with 8M urea or washed with sodium carbonate (pH 11.5). Urea was expected to dislodge proteins that are weakly or peripherally associated with membranes (Figure 5b, scheme 2) (Schaad *et al*., 1997) whereas sodium carbonate renders microsomes into membranous sheets, thus releasing the soluble luminal proteins (Figure 5b, scheme 1) (Peremyslov *et al*., 2004). After treatments with both agents, p7B appeared to be mainly associated with the membranous pellet fraction (Figure 5a), suggesting a tight association with microsomal membranes. To confirm this conclusion, p7B translation reaction mixtures were also treated with Triton X-114, a detergent that forms a separate organic phase to which the membrane lipids and hydrophobic proteins are segregated (Bordier, 1981). Because p7B was detected in the organic, but not the aqueous phase (Figure 5a), we concluded that p7B is an integral membrane protein. Further experiments will be needed to define its topology (Figure 5b, scheme 3).

DISCUSSION

Non-virion cell-to-cell movement of plant carmoviruses involves specific transport of replicated genomes by means of two small movement proteins (DGBp) and in some instances requiring coat protein (Hacker *et al.*, 1992; Li *et al.*, 1998; Cohen *et al.*, 2000; Genoves *et al*., 2006). Although the alignment of carmovirus homolog DGB proteins revealed low identity, similarity of amino acid sequences was noted that mostly affected regions arranged as conserved secondary structure elements. These data suggest that the biological function of both proteins is dependent on the physical and chemical properties of the residues either by itself or by influencing the folding of the polypeptide backbone rather than primary structure. *In vitro* studies have shown that the proteins encoded by the DGB 5'-proximal genes from both TCV and CarMV are able to bind RNA in a sequence non-specificity fashion. However, only CarMV p7 RBD has been well-

characterized and localized to the basic central region of the protein (Wobbe *et al*., 1998; Marcos *et al*., 1999; Vilar et al. 2001, 2005). CarMV p7 RBD consists of an α-helical inducible structure that also includes almost all basic residues of the protein. Both secondary structure and positively charged amino acids modulate RNA binding by means of an RNA:protein adaptative process (Vilar *et al*., 2001, 2005). Moreover, a lysine to glutamate mutation in amino acid position 25 of TCV p8 reduced RNA binding activity and virulence on *Arabidopsis thaliana* (Wobbe *et al*., 1998). The essential role of basic residues in RNA binding has been described for MPs such as TGBp1 (Morozov and Solovyev, 2003) and the 30K superfamily (Herranz *et al*., 2005) from other positive ssRNA virus. Despite the fact that the α-helix is predicted at nearly the same position in all homolog DGBp1, the distribution of basic residues varied considerably and was not always concentrated in the central region as was found for MNSV p7A. Gel-shift assays revealed that p7A can bind ssRNA non-specifically in a slightly cooperative manner as expected. However, when RNA complex formation by full-length p7A and three deletion mutants was tested by Northwestern assays, results revealed that although RNA binding was impaired when the central region was removed, deletion of either the Nt or Ct region also dramatically reduced binding. Unlike the negatively charged Nt from CarMV p7, the Nt from MNSV p7A contains a number of positively charged amino acids (five basic residues conferring an overall charge of +1 *vs* the +3 observed at the central domain). Therefore, the p7A Nt could also participate in RNA-binding as an extension of the basic central RBD. Finally, the lack of the β-sheet Ct domain in the MBP-p7A$\Delta_{45\text{-}65}$ mutant protein could hypothetically affect the cooperative binding of protein molecules prior to fixation onto a solid phase in Northwestern assays or it might influence the correct folding of the rest of the molecule; both of these possibilities could affect the RNA binding. These results are in accordance with the K_d values from gel shift assays using the p7A$_{23\text{-}44}$ peptide and MBP-p7A protein (9 mM *vs* 25.7μM, respectively), which revealed that the central region alone could not account for the RNA-binding properties of the entire p7A protein unlike that observed with CarMV p7 and its RBD derived peptide (K_d values: 0,7 and 1,1μM, respectively) (Marcos *et al*, 1999).

Since nucleic acid binding associated with MPs seems to be a non-sequence specific process, MPs are possibly translated in close proximity to the genome replication complex to bind viral but not host plant RNA. Therefore, the ability of a virus to move is determined by interactions among the genome-MP complex and host proteins from cellular secretory pathways and the cytoskeleton (Nelson and Citovsky, 2005; Scholthof, 2005). In the TGB system, TGBp2 and TGBp3 play this role since they have been described as integral membrane proteins that are associated with the endoplasmic reticulum (ER) (Morozov and Solovyev,

2003; Verchot-Lubicz, 2005). TGBp3 redirects TGBp2 and most likely TGBp1 from the ER network to the plasmodesmata (Haupt *et al*., 2005; Solovyev *et al*., 2000; Zamyatnin *et al*., 2004). In carmoviruses, *in vitro* experiments demonstrated that CarMV p9 is the responsible for the interaction with ER (Vilar et al, 2002 Sauri *et al*., 2005). As with hordei-like and potex-like TGBp3, two- or single-spanning transmembrane domains are predicted for CarMV-like and MNSV-like DGBp2, respectively. Evidence is herein provided that MNSV p7B and most likely all single-spanning transmembrane DGBp2 also insert *in vitro* into the ER lipid bilayer as integral proteins. Therefore, MNSV-like DGBp2 like potex-TGBp3 may be functionally sufficient to direct the intracellular movement of the carmovirus complex DGBp1:RNA. Alternatively, a dimerization process could be involved. In this sense, several cysteine residues that are located at all homolog MNSV-like but not CarMV-like DGBp2 Nt can potentially generate intermolecular covalent disulfide bonds as occurs with the 6-kDa transmembrane protein from closteroviruses (Peremyslov *et al*., 2004). Cysteines are conserved among all sequenced isolates of MNSV except for the residue located at position 4, which was replaced by Tyrosine in five isolates (data not shown). Interestingly, anomalous Cys-Tyr covalent bonds involving protein interactions have been described (Diaz *et al*., 2004).

To conclude, viral genome binding function seems to be accomplish by p7A whereas p7B could be involved in the association with the intracellular membrane system. Both functions have been described for a number of viral MPs. However, the molecular mechanism used to target the MNSV ribonucleoprotein complex to plasmodesmata and then from cell-to-cell in a coat protein-independent process and linked to the p7B silencing suppression (Genoves *et al*., 2006) is still unknown. In this scenario, unlike the 30K family, TGB and other multicomponent transport systems, carmovirus movement based on DGB of MPs is energy-dependent on host proteins. Therefore, this simple system converts such virus into a suitable model of study to advance into the knowledge of mechanisms involved in plant virus cell-to-cell movement and the interactions with host factors produced during the process.

MATERIALS AND METHODS

Expression in bacteria, purification and analysis of MNSV p7A and the deletion mutant forms. MNSV p7A and p7B genes, and the deletion mutant forms p7A$\Delta_{1\text{-}22}$ and p7A$\Delta_{45\text{-}65}$, lacking the amino acid residues located between positions 1-22 (N-terminal region) and 45-65 (C-terminal region) respectively, were amplified from plasmid pMNSV-Al which contains the genomic sequence of the Spanish isolate MNSV-Al (**DQ339157**) (Gosalvez *et al*., 2004; Genoves *et al*., 2006). The PCR products were fused *in frame* after the

coding sequence of maltose binding protein (MBP) into pMal-c2x expression vector (New England Biolabs Inc., MA, USA) to generate the recombinant constructs pMal-7A, pMal-7AΔ_{1-22} and pMal-7A$\Delta_{45-65.}$ Moreover, the central region of p7A encoding residues 23-44 was deleted by reverse PCR of plasmid pMal-7A with phosphorylated oligonucleotides VP 461 and 462 (Table 1). The amplified product was self-ligated to generate plasmid pMal-7AΔ_{23-44}. Alternatively, MNSV p7A gene was cloned into pETDuet-1 (Novagen) by deleting the second T7 promoter and fusing the p7A ORF after a sequence coding for a six histidine tag to generate pET-p7A construct. PCRs were carried out by using Vent DNA polymerase (New England Biolabs Inc., MA, USA) and indicated primer pairs (Table 1). All pMal-p7A constructions as well as pMal-c2x vector were introduced into the *E. coli* strain DH5α by electroporation (GenePulser Xcell™ electroporator system, Bio-Rad). *E. coli* strain BL21 was used in the case of pET-p7A. Next, all recombinant p7A proteins (His-tagged p7A, MBP-p7A, MBP-p7AΔ_{1-22}, MBP-p7AΔ_{23-44} and MBP-p7AΔ_{45-65}) as well as fusion MBP-β-galactosidase α fragment protein (MBP-βgalα) resulting from the pMal-c2x expression vector were purified as manufacturer protocol indicated. The purified proteins were quantified and analyzed by SDS-PAGE in 12 % polyacrylamide gels after Coomassie brillant blue staining.

Synthesis of the RBD-derived peptide and circular dichroism analysis. Synthetic peptide including the p7A amino acid sequence comprised between residues 23 to 44 (p7A$_{23-44}$, Ac-GGKQKNSMGRKIANDAISESKQ-NH_2) was synthesized as previously described (Marcos *et al*, 1999 Secondary structure was monitored by circular dichroism spectroscopy (Jasco J-810 CD spectropolarimeter). CD spectra were the average of a series of ten scans taken at 0.2 nm intervals.

Nucleic acid binding assay. Protein RNA-binding studies were performed by means of electrophoretic mobility shift assay (EMSA) as previously described (Herranz *et al*., 2004). Briefly, 5 ng of a digoxigenin labelled plus-strand MNSV RNA (CP(+) RNA) located on the coat protein ORF (2841-3304 positions) and generated by *in vitro* transcription from BamHI-linearized pMNSV-CP (Gosalvez *et al.,* 2004) by using T3 RNA polymerase, was heat denatured for 5 min at 85ºC and then allowed to cool to room temperature for 15 min. CP (+) RNA was incubated for 30 min at room temperature with different amounts of MBP-βgalα,MBP-p7A, MBP-p7B and His-tagged p7A recombinant proteins as well as with several concentrations of synthetic peptide p7A$_{23-44}$ in a 10 μl reaction mix also containing 10 mM Tris-HCl pH 8.0, 100 mM NaCl, 50 % glycerol and 2 units of RNase inhibitor. Afterwards, samples were electrophoresed on a 1% agarose gel in 1X TAE buffer (40 mM Tris-acetate, 1 mM EDTA, pH 8.0), capillary-transferred to positively-charged nylon membranes (Roche Diagnostics GmbH) in the presence of 10X SSC (1,5M NaCl,

0,15M sodium citrate) and exposed to UV irradiation (700 x 100 μJ/cm2) to cross-link RNA. Riboprobe detection was conducted as previously described (Pallás *et al.,* 1998).

Nucleic acid binding assay in the presence of competitors was performed by mixing the CP(+) RNA with either equal or with ten-fold mass excess of different types of nucleic acids as well as with a constant amount (6 μg) of MBP-p7A recombinant protein. Competitors included: a 20nt-length single strand DNA (ssDNA) oligonucleotide (VP 51-1, TTTACCCACAGTGAAGCTTGC, viral positions 2841 to 2861); a double strand DNA (dsDNA) corresponding to CP(+) RNA sequence obtained by PCR using pMNSV-CP as template and primer pair VP 51-1 and VP 51-2 (TGGATCCGGTAGTAGGAATG, complementary sequence of coat protein positions 3285 to 3304); a 1238nt-length heterologous ssRNA consisting of the complete sequence of the coat protein from *Lettuce big-vein associated virus* (LBVaV) (Navarro *et al*., 2004) and finally, a dsRNA obtained by annealing of non-labelled CP(+) RNA and its complementary RNA sequence CP(-) RNA followed by RNase A/RNase T1 treatment in the presence of 2X SSC.

Additionally, the RNA-binding activity dependence on salt was monitored by increasing the NaCl concentration in EMSA assay using 5ng of CP(+) RNA and 6 μg of MBP-p7A recombinant protein.

Northwestern assays. Recombinant proteins MBP-βgalα, MBP-p7A, MBP-p7A$\Delta_{1\text{-}22}$, MBP-p7A$\Delta_{23\text{-}44}$ and MBP-p7A$\Delta_{45\text{-}65}$ were electrophoresed through 12 % SDS-polyacrylamide gels and electroblotted to nitrocellulose membranes (Bio-Rad) in the presence of transfer buffer (25 mM Tris, 192 mM glycine and 20% methanol). Northwestern-blot assays were performed as described previously (Pallás *et al*., 1999). The membrane-attached proteins were renatured by four-fold shaking incubation for 30 min a room temperature in RN buffer (10 mM Tris-HCl pH7.5, 1 mM EDTA, 100 mM NaCl, 0.05 % Triton X-100, 1X Denhardt´s reagent). Digoxigenin-labelled CP(+) RNA was then added to RN buffer and incubation was continued over night. The membrane was washed three times (15 min each) in the same RN buffer lacking Triton X-100 and Denhardt´s reagent. Finally, bound RNA was detected as described (Pallás *et al.,* 1998) but Tween 20 was omitted from washing solutions and NBT-BCIP colorimetric substrate was used.

***In vitro* transcription and translation of p7B in reticulocyte lysate.** Plasmid pGEM-p7B was created by subcloning p7B sequence into *Nco*I/*Nde*I restriction sites in the pGEM-Lep vector (Nilsson and von Heijne, 1993). *In vitro* transcription was performed as previously reported (Vilar *et al*., 2002). Briefly, the reaction mixtures were incubated at 37 °C for 2 h. The mRNAs were purified using a Qiagen RNeasy clean up kit and verified on 1% agarose gel. *In vitro* translation of the synthesized mRNA was done in the presence of reticulocyte lysate, [^{35}S]Met, and dog pancreas microsomes as described previously (Nilsson and von

Heijne, 1993; Vilar *et al*., 2002). After translation, the samples were analyzed by 20% SDS-PAGE.

Membrane sedimentation, urea treatment, alkaline wash and triton X-114 partitioning. The translation reaction mixture was diluted in either 8 volumes of buffer A (35 mM Tris-HCl at pH 7.4 and 140 mM NaCl) for the untreated samples, 4 volumes of buffer A containing 8 M urea for the urea treated samples, or 4 volumes of buffer A containing 100 mM Na_2CO_3 (pH 11.5) for the alkaline extraction, as previously described (Garcia-Saez *et al*., 2004). The samples were incubated on ice for 30 min, and then clarified by centrifugation at 10.000 *g* and 4 °C for 10 min. Subsequently membranes were collected by layering the supernatant onto a 50 μl sucrose cushion and centrifugation at 100.000 *g* for 20 min at 4 °C in a Beckman tabletop ultracentrifuge with a TLA-45 rotor. Finally, pellets and supernatants were analyzed by 20% SDS-PAGE.

The Triton X-114 partitioning experiments were performed according to (Schaad *et al*., 1997). A total of 10 μL of hydrated Triton X-114 were added to 55 μL of the translation reactions containing microsomes, and the mixtures were incubated for 30 min on ice. The incubated Triton X-114 samples were equilibrated at 37 °C for 10 min to allow for the development of aqueous and organic phases (Bordier, 1981). These phases were then separated by centrifugation at 10.000 *g* at room temperature. Subsequently, the lower, detergent-rich fraction was washed twice by adding 10 volumes of fresh detergent-free buffer, followed by vortexing, incubation on ice for 30 min, and phase separation as before. The proteins present in the aqueous and detergent-rich fractions were finally precipitated in acetone and analyzed by 20% SDS-PAGE.

Acknowledgements

We thank V. Navarro for her technical assistance. This work was supported by Grants BIO05-7331 and GV04B-183 from the grating agency DGICYT and Generalitat Valenciana, respectively. J.A. Navarro and A. Genovés are recipients of an I3P contract and a PhD fellowship from the Consejo Superior de Investigaciones Científicas and the Spanish Ministerio de Educacion y Ciencia, respectively.

REFERENCES

Aparicio, F., Vilar, M., Pérez-Payá, E., Pallás, V., 2003. The coat protein of *Prunus necrotic ringspot virus* specifically binds to and regulates the conformation of its genomic RNA. Virology 313, 213-223.

Bayne, E.H., Rakitina, D.V., Morozov, S.Y., Baulcombe, D.C., 2005. Cell-to-cell movement of *Potato Potexvirus X* is dependent on suppression of RNA silencing. Plant J 44, 471-482.

Bozarth, C.S., Weiland, J.J., Dreher, T.W., 1992. Expression of ORF-69 of *Turnip yellow mosaic virus* is necessary for viral spread in plants. Virology 187, 124-130.

Bordier, C., 1981. Phase separation of integral membrane proteins in Triton X-114 solution. J Biol Chem 256, 1604-1607.

Burd, C.G., Dreyfuss, G., 1994. Conserved structures and diversity of functions of RNA-binding proteins. Science 256, 615-621.

Canizares, M.C., Marcos, J.F., Pallas, V., 2001. Molecular variability of twenty-one geographically distinct isolates of *Carnation mottle virus* (CarMV) and phylogenetic relationships within the Tombusviridae family. Arch Virol 146, 2039-2051.

Carey, J., 1991. Gel retardation. In Methods in Enzymology. Protein-DNA Interactions. pp. 103-117. Edited by R.T. Sauer. Academic Press. San Diego, CA.

Castano A, Hernandez C., 2005. Complete nucleotide sequence and genome organization of *Pelargonium line pattern virus* and its relationship with the family Tombusviridae. Arch Virol 150, 949-65.

Citovsky, V., Knorr, D., Schuster, G., Zambryski, P. 1990. The p30 movement protein of *Tobacco mosaic virus* is a single-strand nucleic acid binding protein. Cell 60, 637-647.

Citovsky, V., Wong, M. L., Shaw, A.L., Venkataram, P.B.V., Zambryski, P., 1992. Visualisation and characterisation of *Tobacco mosaic virus* movement protein binding to single-stranded nucleic acids. Plant Cell 4, 397-411.

Claros, M.G., von Heijne, G., 1994 TopPred II: An improved software for membrane protein structure prediction. CABIOS 10, 685-686.

Cohen, Y., Gisel, A., Zambryski, P.C., 2000. Cell-to-cell and systemic movement of recombinant green fluorescent protein-tagged *Turnip crinkle viruses*. Virology 273, 258-266.

Cserzö, M., Wallin, E., Simon, I., von Heijne, G., Elofsson, A., 1997. Prediction of transmembrane α-helices in prokaryotic membrane proteins: the Dense Alignment Surface method. Protein Engineer 10, 673-676.

Daròs, J.A., Carrington, J.C. 1997. RNA binding activity of NIa proteinase of *Tobacco etch potyvirus*. Virology 237, 327-336.

Diaz, A., Horjales, E., Rudino-Pinera, E., Arreola, R., Hansberg, W., 2004. Unusual Cys-Tyr covalent bond in a large catalase. J Mol Biol 342, 971-985.

Garcia-Saez, A.J., Mingarro, I., Perez-Paya, E., Salgado, J., 2004. Membrane-insertion fragments of Bcl-xL, Bax, and Bid. Biochemistry 43, 10930-10943.

Genoves, A., Navarro, J.A., Pallas, V., 2006. Functional analysis of the five Melon necrotic spot virus genome-encoded proteins. J Gen Virol 87, 2371-2380.

Hacker, D.L., Petty, I.T., Wei, N., Morris, T.J., 1992. *Turnip crinkle virus* genes required for RNA replication and virus movement. Virology 186, 1-8.

Haup, S., Cowan, G.H., Ziegler, A., Roberts, A.G., Oparka, K.J., Torrance, L., 2005. Two plant-viral movement proteins traffic in the endocytic recycling pathway. Plant Cell 17, 164-181.

Heinlein, M., Epel, B.L., 2004. Macromolecular transport and signaling through plasmodesmata. Int Rev Cytol 235, 93-164.

Herranz, M.C., Pallas V., 2004. RNA-binding properties and mapping of the RNA-binding domain from the movement protein of *Prunus necrotic ringspot virus*. J Gen Virol 85, 761-768.

Herranz, M.C., Sanchez-Navarro, J.A., Sauri, A., Mingarro, I., Pallas, V., 2005. Mutational analysis of the RNA-binding domain of the *Prunus necrotic ringspot virus* (PNRSV) movement protein reveals its requirement for cell-to-cell movement. Virology 339, 31-41.

Hull, R., 2002. Virus movement through the plant and effects on plant metabolism. In *Matthews' plant virology*, 4th edn, pp 373-436. Edited by Academic Press, San Diego.

Kasteel, D.T., Wellink, J., Goldbach, R.W., van Lent, J.W. 1997. Isolation and characterization of tubular structures of *Cowpea mosaic virus*. J Gen Virol 78, 3167-3170.

Kawakami, S, Watanabe, Y., Beachy, R.N., 2004. *Tobacco mosaic virus* infection spreads cell to cell as intact replication complexes. Proc Natl Acad Sci U S A 101, 6291-6296.

Krogh, A., Larsson, B., von Heijne, G., Sonnhammer, E.L., 2001. Predicting transmembrane protein topology with a hidden Markov model: application to complete genomes. J Mol Biol 305, 567-580.

Li, W.Z., Qu, F., Morris, T.J., 1998. Cell-to-cell movement of *Turnip crinkle virus* is controlled by two small open reading frames that function in trans. *Virology* 244, 405-16.

Lin K., Simossis V.A., Taylor W.R., Heringa J. 2005. A Simple and Fast Secondary Structure Prediction

Algorithm using Hidden Neural Networks. Bioinformatics. 21, 152-159.

Kawakami, S, Watanabe, Y., Beachy, R.N., 2004. *Tobacco mosaic virus* infection spreads cell to cell as intact replication complexes. Proc Natl Acad Sci U S A 101, 6291-6296.

Li, W.Z., Qu, F., Morris, T.J., 1998. Cell-to-cell movement of *Turnip crinkle virus* is controlled by two small open reading frames that function in trans. Virology 244, 405-16.

Lucas, W.J., 2006. Plant viral movement proteins: agents for cell-to-cell trafficking of viral genomes. Virology 344,169-184.

Marcos, J.F., Vilar, M., Perez-Paya, E., Pallas, V., 1999. *In vivo* detection, RNA-binding properties and characterization of the RNA-binding domain of the p7 putative movement protein from *Carnation mottle carmovirus* (CarMV). Virology 255, 354-365.

Melcher, U., 2000. The '30K' superfamily of viral movement proteins. J Gen Virol 81, 257-266.

Morozov, S.Y., Solovyev, A.G., 2003. Triple gene block: modular design of a multifunctional machine for plant virus movement. J Gen Virol 84, 1351-1366.

Navarro, J.A., Botella, F., Maruhenda, A., Sastre, P., Sánchez-Pina, M.A., Pallas, V. 2004. Comparative infection progress analysis of *Lettuce big-vein virus* and *Mirafiori lettuce virus* in lettuce crops by developed molecular diagnosis techniques. Phytopathology 94:470-477.

Nelson, R.S., Citovsky, V., 2005. Plant viruses. Invaders of cells and pirates of cellular pathways. Plant Physiol 138, 1809-1814.

Nilsson, I., von Heijne, G., 1993. Determination of the distance between the oligosaccharyltransferase active site and the endoplasmic reticulum membrane. J Biol Chem 268, 5798-5801.

Noueiry, A.O., Lucas W.J., Gilbertson, R.L., 1994. Two proteins of a plant DNA virus coordinate nuclear and plasmodesmatal transport. Cell 76, 925-932.

Pallás, V., Más, P., Sánchez-Navarro, J.A., 1998. Detection of plant RNA viruses by non-isotopic dot-blot hybridisation. In: G. Foster and S. Taylor (Eds), Plant Virus Protocols: From Virus Isolation to Transgenic Resistance, Humana Press, Totowa, New Jersey, pp. 461-468.

Pata, J. D., Schultz, S. C., Kirkegaard, K., 1995. Functional oligomerization of poliovirus RNA-dependent RNA polymerase. RNA 1, 466-477.

Peremyslov, V.V., Pan, Y.W., Dolja V.V., 2004. Movement protein of a closterovirus is a type III integral transmembrane protein localized to the endoplasmic reticulum. J Virol 78, 3704-3709.

Pouwels, J., van der Velden, T., Willemse, J., Borst, J.W., van Lent, J., Bisseling, T., Wellink, J., 2004.

Studies on the origin and structure of tubules made by the movement protein of *Cowpea mosaic virus.* J Gen Virol. 85, 3787-3796.

Prokhnevsky, A.I., Peremyslov, V.V., Napuli, A.J., Dolja, V.V., 2002. Interaction between long-distance transport factor and Hsp70-related movement protein of *Beet yellows virus.* J Virol 76,11003-11011.

Sánchez-Navarro, J.A., Herranz, M.C., Pallas, V., 2005. Cell-to-cell movement of *Alfalfa mosaic virus* can be mediated by the movement proteins of Ilar-, bromo-, cucumo-, tobamo- and comoviruses, and does not require virion formation. Virology *in press*

Sauri, A., Saksena, S., Salgado, J., Johnson, A.E., Mingarro, I., 2005. Double-spanning plant viral movement protein integration into the endoplasmic reticulum membrane is signal recognition particle-dependent, translocon-mediated, and concerted. J Biol Chem 280, 25907-25912.

Schaad, M.C., Jensen, P.E., Carrington, J.C., 1997, Formation of plant RNA virus replication complexes on membranes: role of an endoplasmic reticulum-targeted viral protein. Embo J 16, 4049-4059.

Scholthof, H.B., 2005: Plant virus transport: motions of functional equivalence. Trends Plant Sci10, 376-382.

Skuzeski J.M., Morris T.J., 1995. Quantitative analysis of the binding of *Turnip crinkle virus* coat protein to RNA fails to demonstrate binding specificity but reveals a highly cooperative assembly interaction. Virology 210, 82-90.

Solovyev, A.G., Stroganova, T.A., Zamyatnin, A.A. Jr., Fedorkin, O.N., Schiemann, J., Morozov, S.Y., 2000. Subcellular sorting of small membrane-associated triple gene block proteins: TGBp3-assisted targeting of TGBp2. Virology. 269, 13-27.

Thompson, J.D., Gibson, T.J., Plewniak, F., Jeanmougin, F., Higgins, D.G., 1997. The ClustalX windows interface: flexible strategies for multiple sequence alignment aided by quality analysis tools. Nucleic Acids Res 24:4876-4882

Tusnady, G.E., Simon, I., 1998. Principles governing amino acid composition of integral membrane proteins: application to topology prediction. J Mol Biol 283, 489-506.

Hull, R., 2002. Virus movement through the plant and effects on plant metabolism. In *Matthews' plant virology*, 4th edn, pp 373-436. Edited by Academic Press, San Diego.

Vaquero, C., Liao, Y. C., Nähring, J., Fisher, R., 1997. Mapping of the RNA-binding domain of the *Cucumber mosaic virus* movement protein. J Gen Virol 78, 2095-2099.

Verchot-Lubicz J., 2005. A new cell-to-cell transport model for Potexviruses. Mol Plant Microbe Interact 18, 283-290.

Vilar, M., Esteve, V., Pallas, V., Marcos, J.F., Perez-Paya, E., 2001. Structural properties of *Carnation mottle virus* p7 movement protein and its RNA-binding domain. J Biol Chem 276, 18122-18129.

Vilar, M., Sauri, A., Monne, M., Marcos, J.F., von Heijne, G., Perez-Paya, E., Mingarro, I., 2002. Insertion and topology of a plant viral movement protein in the endoplasmic reticulum membrane. J Biol Chem 277, 23447-23452.

Vilar, M., Sauri, A., Marcos, J.F., Mingarro, I., Perez-Paya, E., 2005. Transient structural ordering of the RNA-binding domain of *Carnation mottle virus* p7 movement protein modulates nucleic acid binding. ChemBioChem. 6, 1391-6.

Waigmann, E., Ueki, S., Trutnyeva, K., Citovsky, V., 2004. The ins and outs of nondestructive cell-to-cell and systemic movement of plant viruses. Crit Rev Plant Sci 23, 195-250.

Wobbe, K.K., Akgoz, M., Dempsey, D.A., Klessig, D.F. 1998. A single amino acid change in *Turnip crinkle virus* movement protein p8 affects RNA binding and virulence on *Arabidopsis thaliana*. J Virol 72, 6247-6250.

Wolf, S., Deom, C.M., Beachy, R.N., Lucas, W.J., 1989. Movement protein of *Tobacco mosaic virus* modifies plasmodesmatal size exclusion limit. Science 246. 377-379.

Zamyatnin, A.A. Jr., Solovyev, A.G., Savenkov, E.I., Germundsson, A., Sandgren, M., Valkonen, J.P., Morozov, S.Y. 2004. Transient coexpression of individual genes encoded by the triple gene block of potato mop-top virus reveals requirements for TGBp1 trafficking. Mol Plant Microbe Interact 17, 921-930.

TABLE 1. Sequences and genome positions of each primer pair used for p7A , the corresponding deletion mutant forms and p7B amplification

Product/Vector	Primer	Primer sequence in 5'-3' orientation[†]	Primer position[+]
p7A/pMalc2x	VP 204	ATGCGGATCCATGGACTCTCAACGAACTG (BamHI)	2442-2460
	VP 235	ATGGAAGCTTTAAAAATTAAAGTTAATAG (HindIII)	2620-2638
p7A/pETDuet-1	VP 963	ACGTTGGATCCGATGGACTCTCAACGAACTG (BamHI)	2442-2460
	VP 964	ACGTTGTCGAGCTAAAAATTAAAGTTAATAG (XhoI)	2620-2638
p7A-Δ_{1-22} /pMalc2x	VP 531	ACGTGGATCCGGGGGAAAACAGAAGAACTC (BamHI)	2508-2527
	VP 235	ATGGAAGCTTTAAAAATTAAAGTTAATAG (HindIII)	2620-2638
p7A-Δ_{23-44} /pMalc2x	VP 204	ATGCGGATCCATGGACTCTCAACGAACTG (BamHI)	2442-2460
	VP 532	ACGTAAGCTT**CTA**TTGCTTCGATTCAGAGATAG (HindIII)	2555-2574
p7A-Δ_{45-65} /pMalc2x	VP 461	P-GCTGTCACCACGTTCTTTAC	2488-2507
	VP 462	P-GGAGTTATGGGTGCCAGCAC	2574-2593
p7B/pMalc2x	VP 216	ATGCGGATCCATGGCTTGTTGCCGTTGTG (BamHI)	2643-2661
	VP 236	ATGCAAGCTTTTAACCATCGCCATTTGTAG (HindIII)	2809-2828

[+] Primer position was numbered after the GenBank of the National Center for Biotechnology Information (**DQ339157)** for MNSV-AI sequence.

[†] The underlined sequences are restriction sites indicated at the end of primer sequence. Boldface sequence corresponds to an introduced stop codon.

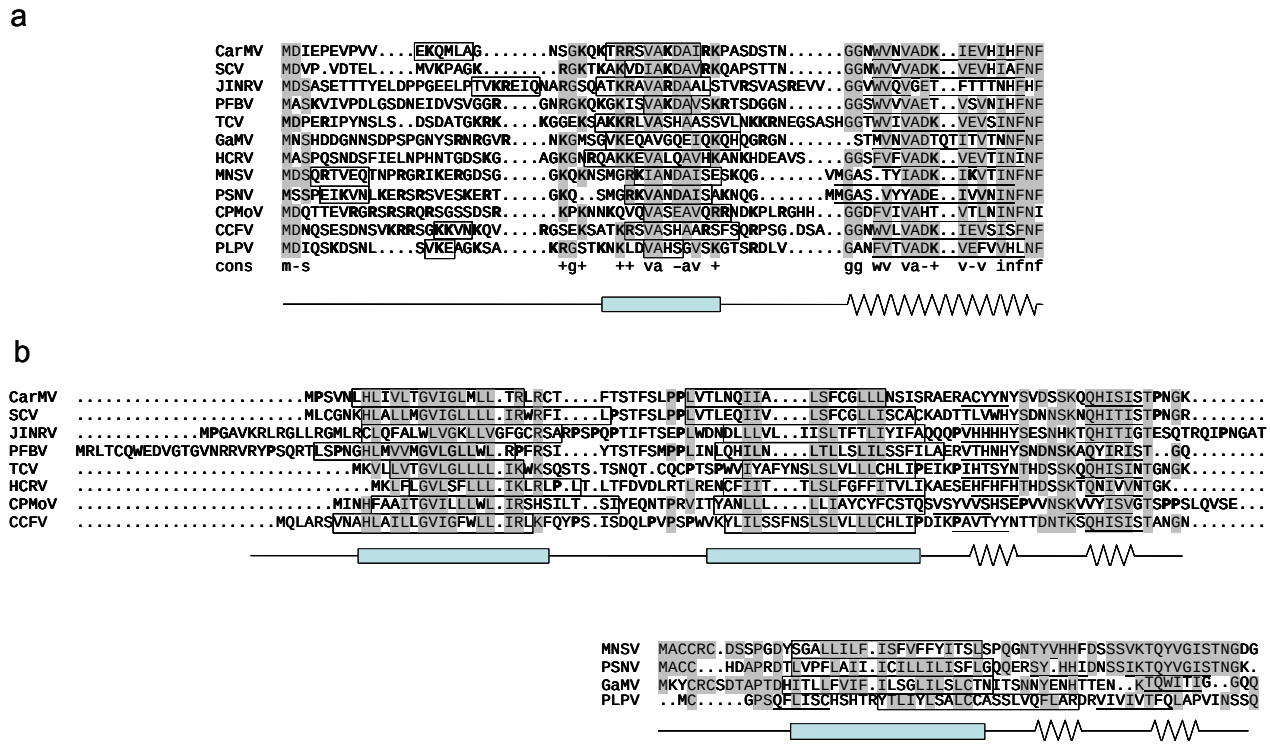

Figure1. (a) Amino acid alignment of the sequences from eleven Carmovirus and related *Pelargonium line pattern virus* (PLPV) DGBp1, CarMV-like (b, up) and MNSV-like (b, down) DGBp2. Consensus residues predicted to be involved in α-helix or transmembrane fragments are boxed in (a) and (b), respectively, whereas β-sheet structured domains are underlined. Amino acid similitude is indicated by grey boxes and basic (K or R) or proline (P) residues are in bold in (a) and (b), respectively. Symbols + and - in consensus sequence represent basic (K or R) and acid residues (D or E), respectively. A diagrammatic representation of deduced secondary structure of DGBps is displayed below each alignment. Boxes represent α-helix or transmembrane fragments in (a) and (b), respectively and broken lines correspond to β-sheets structures. CarMV, *Carnation mottle virus* (**X02986**); SCV, *Saguaro cactus virus* (**U72332**); JINRV, *Japanese iris necrotic ring virus* (***D86123***); PFBV, *Pelargonium flower break virus* (**AJ514833**); TCV, *Turnip crinkle virus* (**M22445**); GaMV, *Galinsoga mosaic virus* (**Y13463**); HCRV, *Hibiscus chlorotic ringspot virus* (**X86448**); MNSV, *Melon necrotic spot virus* (**DQ339157**); PSNV, *Pea stem necrosis virus* (**AB086951**); CPMoV, *Cowpea mottle virus* (**U20976**); CCFV, *Cardamine chlorotic fleck virus* (**L16015**)

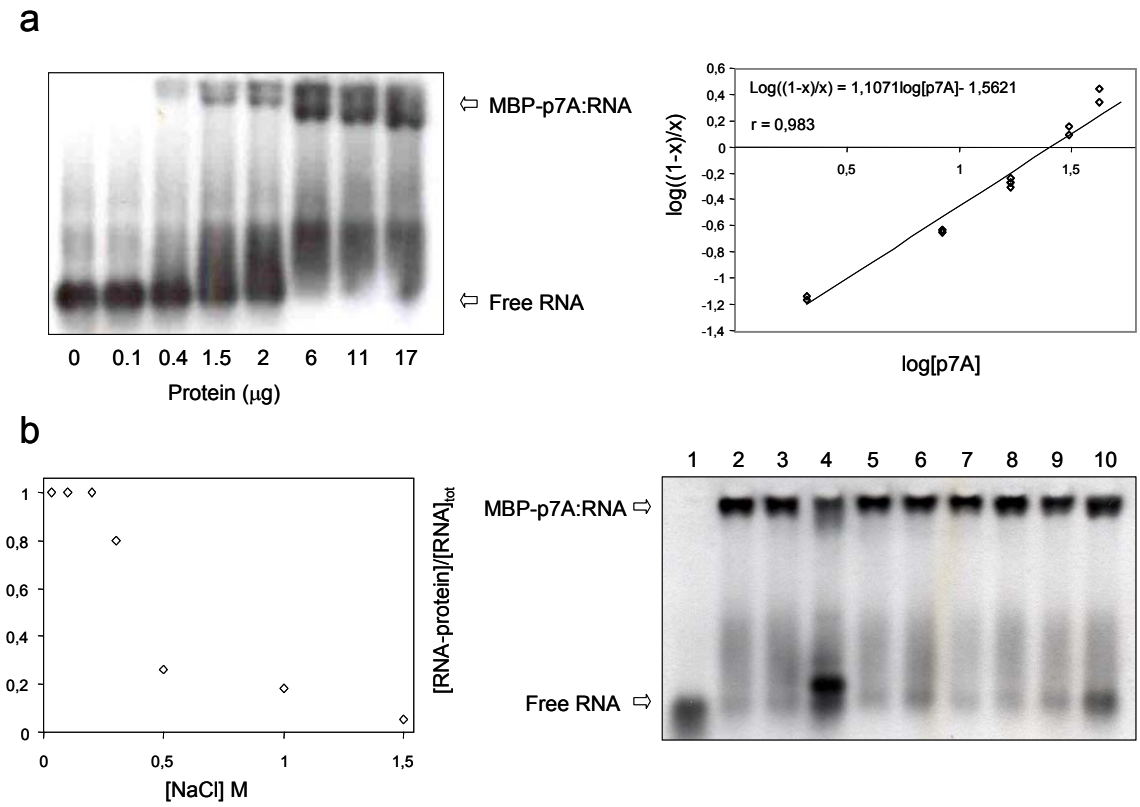

Figure 2. Determination of the *in vi*tro RNA binding properties of the recombinant MBP-p7A. a) Analysis of MBP-p7A binding to ssRNA (CP (+) RNA) by electrophoretic mobility shift assays (EMSA) (left) and study of binding kinetics by means of a Hill transformation of data from three independent EMSA (right). Equation of linear regression and the corresponding r coefficient are indicated into the graphic representation. b) Dependence of MBP-p7A RNA-binding activity on salt concentration represented as the fraction of bound RNA against NaCl concentration (left) and ssRNA binding specificity (right) measured by EMSA in the absence (lane 2) and presence (lanes 3 to 10) of either equal (odd lanes) or ten-fold (even lanes) mass excess of different classes of competitors: heterologous ssRNA (lanes 3 and 4) and homologous dsRNA (lanes 5 and 6), ssDNA (lanes 7 and 8) and dsDNA (lanes 9 and 10). Lane 1 corresponds to electrophoretic mobility of the ssRNA probe in the absence of MBP-p7A.The position of free and protein bound RNA on EMSA are marked.

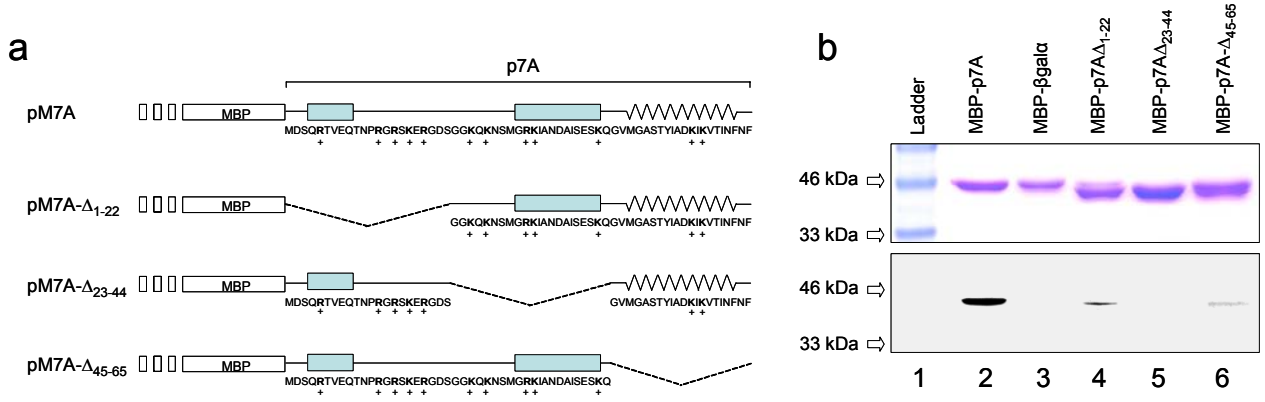

Figure 3. Characterization of the RNA binding domain (RBD) of p7B a) Diagrammatic representation of the pMal-7A and its mutant forms pMal-7A$\Delta_{1\text{-}22}$, pMal-7A$\Delta_{23\text{-}44}$ and pMal-7A$\Delta_{45\text{-}65}$. Numbers in the construct name and discontinuous lines in diagram refer to the amino acid residue position deleted from wild-type protein. Grey boxes and broken line represent α-helix and β-sheets structures, respectively. Symbols + indicated the position of basic residues (K or R). b) SDS-PAGE analysis of the purified MBP-βgalα, MBP–p7A and its deleted forms in a 12 % gel stained with Coomassie blue (up) and the corresponding ssRNA binding analysis by Northwestern blot assay (down). The positions of the molecular mass markers are indicated on the left.

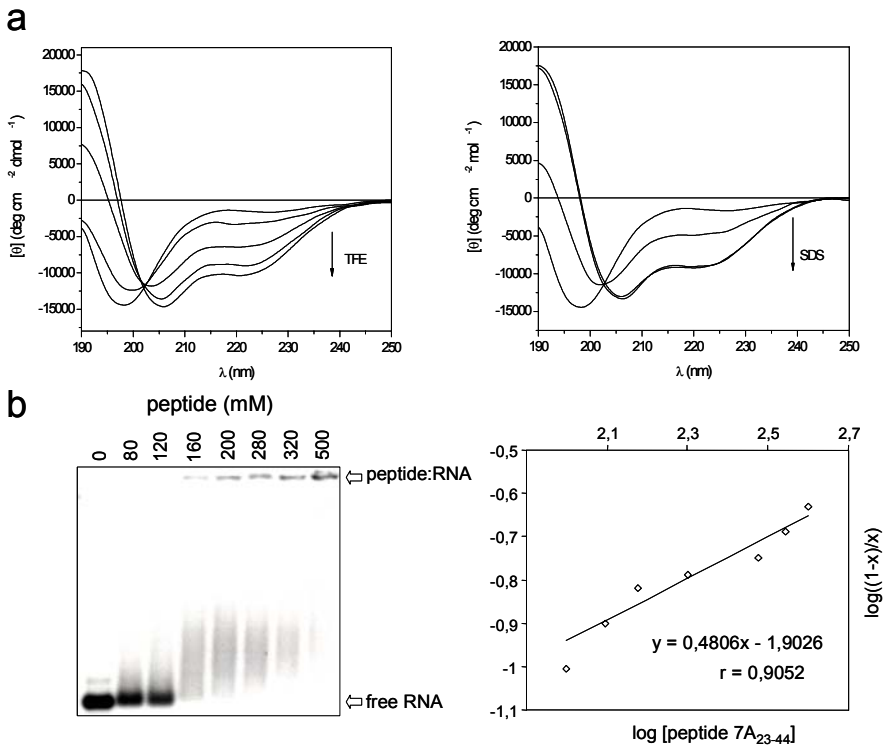

Figure 4. a) Far UV CD spectra of RBD-derived peptide p7A$_{23-44}$ in the presence of increasing concentrations of two different secondary structure inductors, TFE (20, 40 60 and 70%, as the arrow indicates) and SDS (1, 5 and 10 mM). Peptide concentration was 30 μM in 5 mM MOPS/NaOH buffer, pH 7.0 at 25ºC. b) RNA-binding analysis of different amount of peptide p7A$_{23-44}$ by EMSA (left) and Hill transformation of data (right). Equation of linear regression and the corresponding r coefficient are indicated.

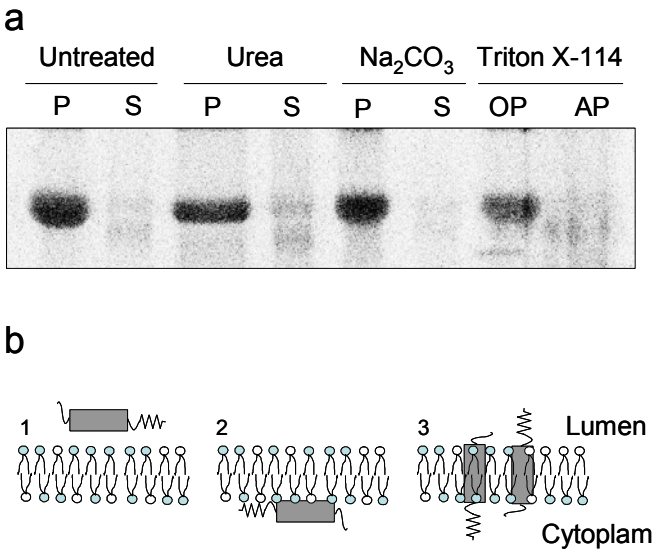

Figure 5. Location in dog pancreas microsomes of p7B protein transcribed/translated *in vitro* a) Segregation of [^{35}S]Met labelled p7B into membranous fraction after urea treatment, alkaline wash (sodium carbonate buffer) and triton X-114 partitioning. P and S, pellet and supernatant, respectively; OP and AP, organic and aqueous phases, respectively. b) Representation of the different membrane association possibilities of p7B with microsomes as luminal (1) and either peripheral (2) or integral (3) membrane-anchored protein.

TABLE 1. Sequences and genome positions of each primer pair used for p7A and the corresponding deletion mutant forms amplification

Product	Primer	Primer sequence in 5'-3' orientation[†]	Primer position[+]
p7A	VP 204	ATGCGGATCCATGGACTCTCAACGAACTG (BamHI)	2442-2460
	VP 235	ATGGAAGCTTTAAAAATTAAAGTTAATAG (HindIII)	2620-2638
p7A-Δ_{1-22}	VP 531	ACGTGGATCCGGGGGAAAACAGAAGAACTC (BamHI)	2508-2527
	VP 235	ATGGAAGCTTTAAAAATTAAAGTTAATAG (HindIII)	2620-2638
p7A-Δ_{23-44}	VP 204	ATGCGGATCCATGGACTCTCAACGAACTG (BamHI)	2442-2460
	VP 532	ACGTAAGCTT**CTA**TTGCTTCGATTCAGAGATAG (HindIII)	2555-2574
p7A-Δ_{45-65}	VP 461	P-GCTGTCACCACGTTCTTTAC	2488-2507
	VP 462	P-GGAGTTATGGGTGCCAGCAC	2574-2593

[+] Primer position was numbered after the GenBank of the National Center for Biotechnology Information (**DQ339157** for MNSV-Al sequence)

[†] The underlined sequences are restriction sites indicated at the end of primer sequence. Boldface sequence corresponds to an introduced stop codon.

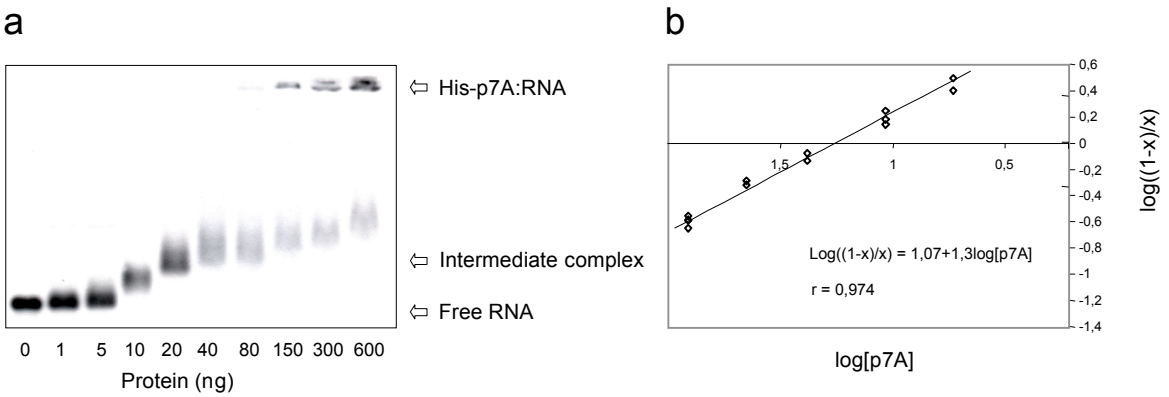

Supplementary figure 1. Determination of the *in vi*tro RNA binding properties of the recombinant His-p7A. Analysis of His-p7A binding to ssRNA (CP (+) RNA) by electrophoretic mobility shift assays (EMSA) (a) and binding kinetics determined by Hill transformation of data from three independent EMSA (b). The position of free and protein bound RNA on EMSA are marked. Equation of linear regression and the corresponding r coefficient are indicated into the graphic representation.

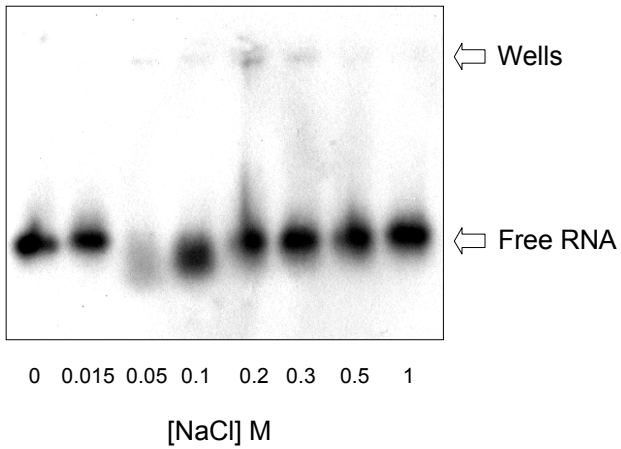

Supplementary figure 2. Mobility shift assays of CP (+) RNA in the presence of MBP-p7B using different NaCl concentrations. The position of free RNA and gel wells on EMSA are marked.